IEEE Access
Multidisciplinary ⋮ Rapid Review ⋮ Open Access Journal

Received March 26, 2020, accepted April 7, 2020, date of publication May 4, 2020, date of current version May 20, 2020.

Digital Object Identifier 10.1109/ACCESS.2020.2991984

Multi-Time Scale Regional Autonomous Operation Strategy for Multi-Microgrids With Three-Phase/Single-Phase Hybrid Structure

ZHUOLI ZHAO[1,3], (Member, IEEE), ZHIRONG XU[2,3], (Student Member, IEEE), JUNTAO GUO[1], PING YANG[3], (Member, IEEE), AND LOI LEI LAI[1], (Fellow, IEEE)

[1]School of Automation, Guangdong University of Technology, Guangzhou 510006, China
[2]China Resources Power Holdings Company Ltd., Shenzhen 518001, China
[3]Guangdong Key Laboratory of Clean Energy Technology, South China University of Technology, Guangzhou 510640, China

Corresponding authors: Zhirong Xu (xuzhirong6@crpower.com.cn) and Ping Yang (eppyang@scut.edu.cn)

This work was supported in part by the National Natural Science Foundation of China under Grant 51907031, in part by the National High Technology Research and Development Program of China (863 Program) under Grant 2014AA052001, and in part by the Operation Fund of Guangdong Key Laboratory of Clean Energy Technology under Grant 2017B030314127.

ABSTRACT In the case of islanding from the distribution network, problems such as source-load power loss under multi-zone island isolation will challenge the autonomous operation of multi-microgrids with three-phase/single-phase hybrid structure. In order to make full use of the resources in the multi-microgrids to realize the reliable and efficient operation of the system as a whole, this paper proposes a multi-time scale regional autonomous control strategy for multi-microgrids with three-phase/single-phase hybrid structure. The dynamic update islanding combination is controlled by the hourly dynamic island combination and the simultaneous search switching to achieve the overall resource allocation optimization. The source-storage-load power and state redistribution are dynamically realized through minute-level centralized coordination and optimization, so that the constraints of the three-phase unbalance are met and the source-load shedding are minimized. The power fluctuations of the sources and loads within each sub-microgrid are suppressed by using the second-level off-grid real-time power control. Moreover, the tie-line power can be maintained as the original given value and the three-phase unbalance degree index can be achieved. The multi-microgrids model with three-phase/single-phase hybrid structure based on DIgSILENT platform is used to verify the correctness and effectiveness of the proposed strategy.

INDEX TERMS Multi-microgrids, multi-time scale, autonomous operation, coordinated control, three-phase/single-phase hybrid structure.

I. INTRODUCTION

Along with the new urbanization and low-carbon energy transformation, microgrids can not only meet the growing demand for users but also promote local consumption of renewable energy [1], [2]. With the large-scale popularization of microgrids [3], the coexistence of the three-phase microgrids and the single-phase microgrids with multiple phase sequences in an adjacent area gradually forms multi-microgrids (MMGs) with three-phase/single-phase hybrid structure [4]. Through synergistic interaction, the new-type multi-microgrids can further improve the reliability, stability and economy of the electricity consumption of users in the region [5]. Also, it is conducive to the high-permeability comprehensive utilization of renewable energy and becomes an essential carrier for the structural reform of the supply side in the energy sector [6].

At present, the analysis and operation of isolated microgrid have been extensively studied. The modeling and stability analysis of a single inverter-dominated microgrid based on eigenvalue theory have been reported in [7]. Dynamic phasor model is established in [8] to predict the stability of the microgrid system. Authors of [9] introduce a multiple-time-scales hierarchical control strategy to ensure the frequency stability for island microgrid. In [10], a centralized control architecture is proposed for small-scale microgrid based on multiple

The associate editor coordinating the review of this manuscript and approving it for publication was Seyyed Ali Pourmousavi Kani.

supervisory control tasks. In [11], a decentralized power management strategy combining bus-signaling and droop control method is adopted to coordinate different distributed generations in an isolated microgrid. In [12], a two-stage robust model is proposed for the resilient operation of microgrids considering the management of frequency deviations and minimization of operation cost. In [13], authors present a stochastic risk-constrained framework for short-term optimal operation of isolated microgrid considering uncertainties of supply and demand side. For multi-microgrids, it will face greater challenges when it islands from the distribution network [14]. The biggest problem which restricts the safe and efficient operation of multi-microgrids is how to make full use of internal source-load-storage in each sub-microgrid for coordinated control, especially when the source-load fluctuations are significant [15].

Recently, some literature has studied the safe and efficient operation of multi-microgrids. In [16], a bilevel programming framework is proposed to analyze the hierarchical decision-making competition among energy services providers in managing multiple microgrids. In [17], the distribution network is considered as coupled microgrids, and a cost-effective optimal control algorithm is presented using coordinated information and schemes among the microgrids. Considering the energy trading between the microgrid and the distribution network, a random probability model for renewable energy resources and load demand is established in [18] to obtain the optimal economical operation solution. In [19], an energy management strategy is developed for cooperative microgrids based on a stochastic predictive control framework. In [20], a two-level stochastic energy management strategy is introduced for the operation of networked microgrids considering the effects of uncertainty in endogenous and exogenous sources. A coordinated and optimized approach for implementing energy management in MMGs is studied in [21]. And a novel probabilistic index is developed to assess the effectiveness of the energy management scenarios. In [22], a multi-step optimization method based on multi-agent system is introduced to determine various available options and ensure the reduction in the operational cost of the MMGs system. In [23], to enhance the resilience of a distribution network composed of MMGs under unexpected disaster events, a hierarchical outage management strategy is proposed. Based on a general framework for reliability evaluation, appropriate hierarchical and centralized and management strategies are developed to enhance the reliability of an MMG distribution system in [24].

The power coordinated management and control of the multi-microgrids are performed through distributed approaches in [25]–[27]. In [25], in order to encourage fair benefit sharing and active energy trading, the Nash bargaining theory is adopted to developed an incentive mechanism for the interactions among the interconnected microgrids. A two-step distributed algorithm based on dual decomposition is introduced in [26] to achieve energy trading between two islanded microgrids. In [27], a two-level hierarchical optimization approach for energy management of microgrid community is presented, in which the upper level is in charge of the operation of the individual microgrid, and the lower level is responsible for the management of the devices of the microgrid community.

However, the above-mentioned control strategy only performs coordinated control for a single microgrid or the same phase sequence multi-microgrids. The existence of single-phase sources, loads and storages causes the three-phase unbalance problem in the three-phase/single-phase hybrid multi-microgrids. The multi-time scale coordinated optimization control of the single-phase and three-phase microgrid interconnections according to the constraints of the three-phase unbalance of the multi-microgrids system are not reported in current literature.

Compared with existing related research, this paper is different and has some improvements in some aspects. The comparison of contributions between this paper and related literature is summarized in Table 1.

Motivated by the aforementioned research gap, this paper proposes a multi-time scale regional autonomous control strategy for a single/three-phase hybrid structure multi-microgrids. First, the hour-level dynamic island switching control is implemented by the regional microgrid central controller hourly to split the regional multi-microgrids into islands. And the islanding optimization and switching are completed by transmitting the combined result of the island division to the central controller of the microgrid, thereby coordinated mutual assistance and overall resource optimal configuration can be achieved by sharing spare capacity. Second, in the minute-level centralized coordination and optimization, the underlying operational information is uploaded through the microgrid central controller. Taking into account the operation of the source-load equipment within the allowable range of three-phase unbalance degree, decisions are made to minimize the abandoned photovoltaic (PV) and load shedding and determine the tie-line power reference of the sub-microgrids. Third, in second-level single microgrid power control, the sub-microgrid source-load storage operation information is collected through the microgrid central controller in real time. Based on off-grid real-time power control strategy, the source-storage power regulation is achieved within its own stability margin. Also, the fluctuations of the PV power generation and load power is stabilized, while ensuring that the three-phase unbalance of the system meets the operational requirements.

The main contributions of this paper are highlighted as follows:

1) Proposing a multi-time scale regional autonomous control strategy suitable for the reliable and efficient operation of the multi-microgrids with three-phase/single-phase hybrid structure.

2) A comprehensive multi-index evaluation model for multi-microgrids island operation is established. And the

TABLE 1. Comparison of contributions between this paper and related literature.

Reference	Optimal operation of single microgrid	Optimal operation of multi-microgrids	Consider three-phase unbalance control in the three-phase/single-phase hybrid multi-microgrids	Multi-time scale operation	Dynamic islanding combination control of multi-microgrids	Autonomous operation of multi-microgrids	Consider the modeling of the uncertainty	Consider power limits and SoC characteristics of ESS operation
[9]	√			√				√
[10], [11]	√							√
[12]	√						√	√
[13]	√						√	
[14], [15]		√				√		
[16], [25]	√	√						
[17], [18]	√	√					√	
[19], [20]	√	√					√	√
[21]	√	√					√	
[22]	√	√						√
[23], [24], [27]	√	√				√		√
[26]	√	√				√		
Proposed Strategy	√	√	√	√	√	√		√

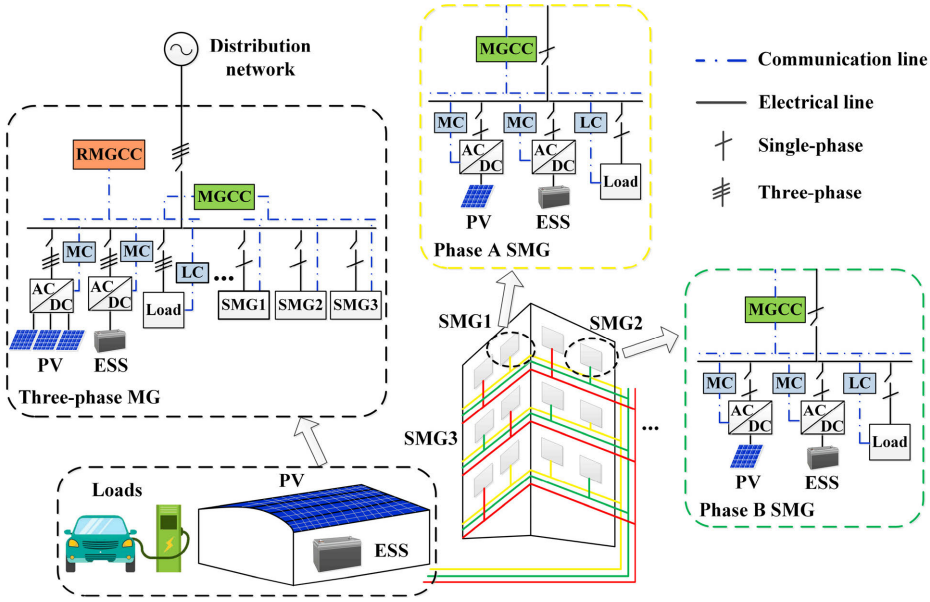

FIGURE 1. The physical topology and the communication network topology of the three-phase/single-phase hybrid multi-microgrids.

overall dynamic optimized island combination and splitting of the three-phase/single-phase hybrid multi-microgrids is realized by the hour-level dynamic islanding strategy.

3) In the context of multi-microgrids with three-phase/single-phase hybrid structure, the constraints of the three-phase unbalance are considered and the source-load shedding are minimized in the proposed minute-level centralized coordination and optimization scheme.

4) By using the developed second-level real-time power control, the power fluctuations of the sources and loads within each sub-microgrid are suppressed, and the three-phase unbalance degree index control can be achieved.

The remainder of this paper is organized as follows. Section II gives the structure of the three-phase/single-phase hybrid multi-microgrids. The multi-time scale regional autonomous coordinated control strategy for the multi-microgrids is presented in Section III. Section IV shows the performance of the three-phase/single-phase hybrid multi-microgrids to verify the effectiveness of the proposed multi-time scale regional autonomous coordinated control strategy. Finally, the conclusion is given in Section V.

II. THREE-PHASE/SINGLE-PHASE MULTI-MICROGRIDS STRUCTURE

The structure of the three-phase/single-phase multi-microgrids system is shown in Fig. 1, which consists of a two-layer microgrid. The upper layer sub-microgrid is a three-phase structure, which is used to simulate the

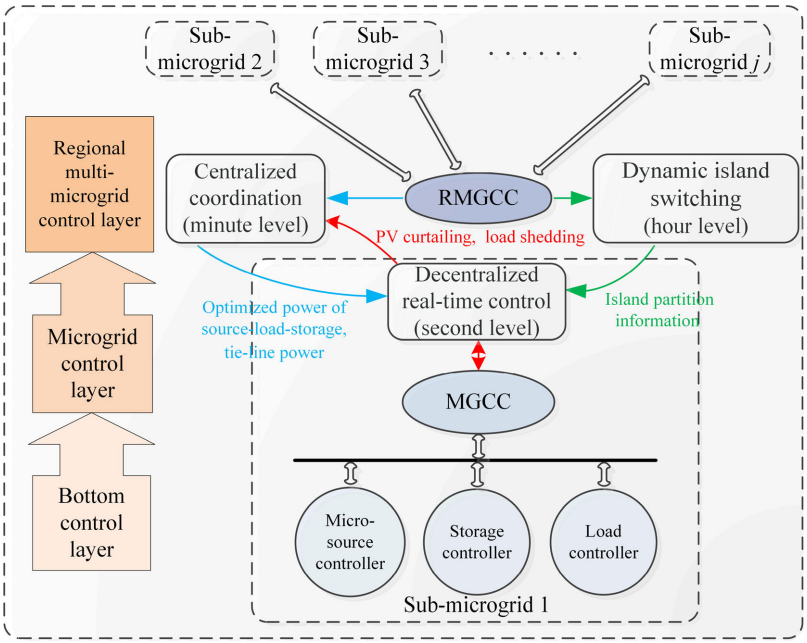

FIGURE 2. Proposed multi-time scale regional autonomous coordinated control architecture of the three-phase/single-phase hybrid multi-microgrids.

three-phase part of the residential-area type multi-microgrids, including three-phase PV, three-phase energy storage system (ESS) and three-phase loads. The lower sub-microgrid is a single-phase structure used to simulate the single-phase home user type microgrid, including single-phase PV, single-phase ESS and single-phase loads. The single-phase sub-microgrid accesses each phase bus of three-phase sub-microgrid through isolating switches.

The microgrid control system based on hierarchical architecture is divided into three layers according to the response speed, time scale and communication requirements. The first layer of control consists of a regional microgrid central controller (RMGCC), which is responsible for regulating the entire multi-microgrids and ensuring the safe and stable operation and power balance of the multi-microgrids. The second layer consists of a microgrid central controller (MGCC), which is responsible for the implementation of control functions within each microgrid. The third layer is the bottom control layer, which is composed of micro-source controllers and load controllers. The proposed control system does not need to set up a server-based microgrid control system, but distributes most of the functional modules to each controller. Moreover, the control system can operate at low cost and in a decentralized manner, and only transmits necessary information to regional coordinated control.

III. MULTI-TIME SCALE REGIONAL AUTONOMOUS COORDINATED CONTROL STRATEGY FOR THREE-PHASE/SINGLE-PHASE MULTI-MICROGRIDS

As shown in Fig. 2, the proposed three-layer multi-time-scale regional autonomous coordinated control architecture consists of second-level decentralized control, minute-level centralized coordination and hour-level dynamic islanding.

The control process is as follows:

(1) Dynamic islanding switching control is performed by RMGCC every hour to achieve the islanding division of regional multi-microgrids. Thus, spare capacity can be shared to support adjacent microgrid, or sub-microgrid that affects the stable operation of the system can be isolated. Also, the optimal allocation of overall resources can be implemented. The dynamic island division result is transmitted to the MGCC to complete the island switching through adjusting the tie-line power with decentralized control.

(2) RMGCC performs centralized coordination optimization every five minutes. The MGCC uploads the bottom operational information, including real-time power, abandoned PV power and load-shedding power. Considering the utilization rate of renewable energy and the supply reliability of load power, the tie-line power command of the sub-microgrid is updated within the allowable range of three-phase unbalance degree. In this way, abandoning renewable energy and load shedding can be avoided.

(3) MGCC collects the operation information of the source, load and storage of the sub-microgrid in real time. Based on the off-grid real-time power control strategy, power regulation of the source, load and storage can be realized within its own stability margin. Thus, the fluctuations of the PV power generation and load power can be stabilized, and the three-phase unbalance degree of the system is guaranteed to meet the requirements.

A. SECOND-LEVEL REAL-TIME POWER CONTROL OF THE SUB-MICROGRID

After the optimized decision, the tie-line power can be compared to a constant load or a constant power supply. In order to ensure the global demand for the established tie-line power

TABLE 2. The charge and discharge power limits of ESS in different intervals.

State interval	SoC range	Charge and discharge power limits of ESS
State interval 1	$(0\sim SoC_{min\,1})$	$[P_{ch},0]$
State interval 2	$(SoC_{min\,1}\sim SoC_{min\,2})$	$[P_{ch},\min\{P_{dis},\frac{SoC-SoC_{min1}}{SoC_{min2}-SoC_{min1}}P_{dis}\}]$
State interval 3	$(SoC_{min\,2}\sim SoC_{max\,2})$	$[P_{ch},P_{dis}]$
State interval 4	$(SoC_{max\,2}\sim SoC_{max\,1})$	$[\max\{P_{ch},\frac{SoC_{max1}-SoC}{SoC_{max1}-SoC_{max2}}P_{ch}\},P_{dis}]$
State interval 5	$(SoC_{max\,1}\sim 1)$	$[0,P_{dis}]$

task, the fixed tie-line power control needs to be realized. To stabilize the power supply and load power fluctuations, and ensure the safe and reliable operation of the energy storage equipment, each sub-microgrid controller implements autonomous second-level decentralized control of the sub-microgrid. Real-time control only needs to transmit data to MGCC by the bottom control layer; thus, the response speed is fast, and the time scale is small. Nevertheless, when the self-adjustment cannot be performed within the stability margin, it is necessary to adopt PV-curtailing or load shedding, which is not conducive to the full utilization of renewable energy and power supply reliability.

To ensure that the ESS always has adjustable margin to stabilize the passive instantaneous tie-line power fluctuation, and also avoid shortened life due to overcharge and over discharge, the state of charge (SoC) of the ESS is divided into five intervals by setting four threshold values. As listed in Table 2, the charge and discharge power limits will be adjusted in different intervals to ensure the safe and flexible operation of the ESS.

P_{ch} and P_{dis} represent the maximum charge and discharge power, respectively. The state interval 1 ($0 \sim SoC_{\min\,1}$) is the emergency lower limit state, in which the SoC of the ESS is extremely low, and can only receive the charging command of the sub-microgrid control layer to absorb energy. The state interval 2 ($SoC_{\min\,1} \sim SoC_{\min\,2}$) is the over-discharge alarm state, in which the remaining capacity of the ESS is insufficient, and the discharging power needs to be limited. The state interval 3 ($SoC_{\min\,2} \sim SoC_{\max 2}$) is the normal state, that is, the ESS can normally charge and discharge in response to the command of the sub-microgrid control layer. The state interval 4 ($SoC_{\max 2} \sim SoC_{\max 1}$) is the overcharge alarm state, that is, the remaining energy of the ESS is large, and the charging power needs to be limited. The state interval 5 ($SoC_{\max 1} \sim 1$) is the emergency upper limit state, that is, the ESS has an extremely large amount of electricity, and can only receive the discharge command from the sub-microgrid control layer to release energy. In this paper, $SoC_{\min\,1}$, $SoC_{\min\,2}$, SoC_{max1} and SoC_{max2} are set to 20%, 40%, 60% and 80%, respectively.

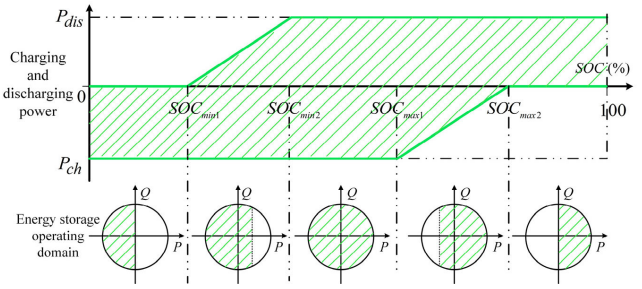

FIGURE 3. Power characteristics and operating region of ESS based on SoC partition.

Considering the charging and discharging active power characteristic of SoC intervals, the ESS operation domain of PQ Cartesian coordinate system is established according to the rated capacity constraints of the ESS converter. The partitioning scheme is the ESS operation domain corresponding to different SoC intervals, as shown in Fig. 3. Hence, the charging and discharging reactive power characteristics and constraints of the ESS considering SoC partition are determined.

According to the above state partitioning scheme, the corresponding charging and discharging power interval in the real-time SoC state of the *i*th ESS can be obtained. Then the ESS operation region of the regional multi-microgrids can be calculated. The power balance equation in the regional multi-microgrids system is satisfied as follows:

$$\sum \bar{S}_{bs} + \bar{S}_{tie} = -\sum \bar{S}_{PV} - \sum \bar{S}_{Ld} = \bar{S}_{net} \tag{1}$$

where $\bar{S}_{bs}$, $\bar{S}_{PV}$ and $\bar{S}_{Ld}$ are the complex power of ESS, PV and load; $\bar{S}_{tie}$ is the complex power of multi-microgrids system tie lines, which is a fixed value constant in a certain period of time, and is the power distribution after the minute-level centralized optimization decision; $\bar{S}_{net}$ is real-time net power.

Based on the idea of approximate off-grid for tie-line power, the generalized energy storage operation region is proposed. The tie-line power is considered based on the energy storage operation region of the sub-microgrid system. To ensure the generalized energy storage operation domain always has a margin, a 10% adjustable margin in the implementation of the source-load-storage coordinated control strategy is considered.

$$\begin{cases} \bar{S}_{\min} = 90\% \times (\sum \bar{S}_{\min\_i} + \bar{S}_{\text{tie}}) \\ \bar{S}_{\max} = 90\% \times (\sum \bar{S}_{\max\_i} + \bar{S}_{\text{tie}}) \end{cases} \tag{2}$$

where $\bar{S}_{\max}$ and $\bar{S}_{\max}$ are the upper and lower limits of the generalized energy storage operation domain; $\bar{S}_{\max\_i}$ and $\bar{S}_{\min\_i}$ are the upper and lower limits of the energy storage operation domain of the *i*th ESS in the sub-microgrid system.

As shown in Fig. 4, the generalized energy storage operation domain $\{\bar{S}_{\min}, \bar{S}_{\max}\}$ is transferred from the energy storage operation domain based on the tie-line power. In the PQ coordinate system, the center of the generalized energy

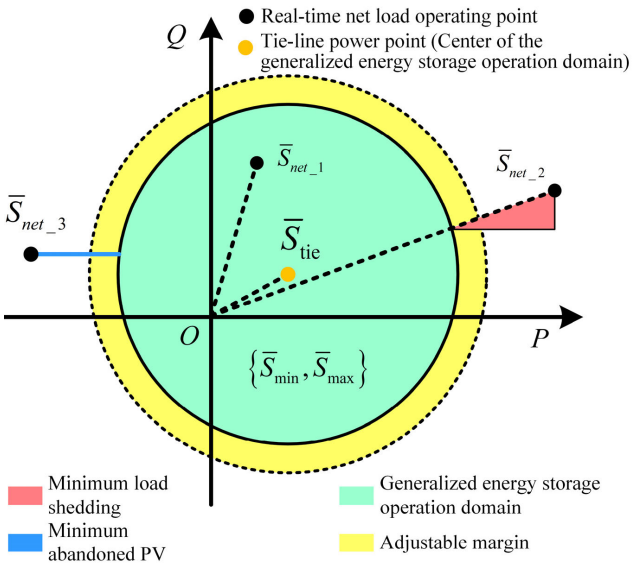

FIGURE 4. The source-load-storage coordinated control diagram based on generalized energy storage operation domain.

storage operation domain is the tie-line power coordinate, and the size of the operation domain remains unchanged before and after the transfer.

The coordinate corresponding to the real-time net load power on the PQ coordinate axis is called the real-time net load operation point. The source-load-storage coordinated control strategy based on the generalized energy storage operation domain is as follows:

(1) As shown in $\bar{S}_{net\_1}$ in Fig. 4, if the real-time net load operating point is included in the generalized energy storage operating domain, it means that the instantaneous power fluctuations of the load and the PV can be stabilized only using the self-regulation of the ESS, that is, equation (1) is satisfied.

(2) If the real-time net load operating point is not included in the generalized energy storage operating domain, it means that the real-time fluctuation of the source-load cannot be stabilized by relying solely on the ESS itself. To avoid long-term and large-scale power deviation of the tie line, the sub-microgrid must adopt the PV-curtailing or load shedding measures to transfer the deviated real-time net load power to the generalized energy storage operation domain. It can be converted into the shortest path problem from the real-time net operation point to the generalized energy storage operation domain, that is, the minimum amount of PV-curtailing or load shedding. As shown in Fig. 4, taking the SoC of the ESS in the normal state interval as an example. If the real-time net operation point $\bar{S}_{net\_2}$ is on the right side of the generalized energy storage operation domain $\{\bar{S}_{min}, \bar{S}_{max}\}$, load shedding is needed to implement; and if $\bar{S}_{net\_3}$ is on the left side of $\{\bar{S}_{min}, \bar{S}_{max}\}$, PV-curtailing is required to perform. PV curtailing or load shedding should follow two principles: 1) Only consider the active power of the PV is adjustable; 2) Considering the discrete characteristics of the switchable load, match and optimize the load in the sub-microgrid according to the minimum load shedding calculated based on the generalized energy storage operation domain.

In summary, the flowchart of the source-load-storage coordinated control scheme based on generalized energy storage operation domain is shown in Fig. 5 and can be described as follow:

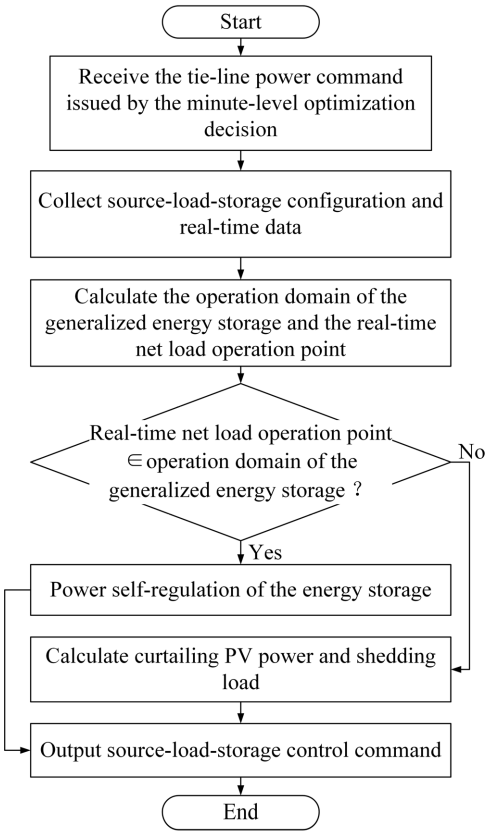

FIGURE 5. Coordinated control flowchart based on generalized energy storage operation domain.

Step 1: The tie-line power of each sub-microgrid according to the centralized coordination and optimization is selected as the initial data input of the fixed tie-line power control.

Step 2: The RMGCC collects the configuration information and the real-time power of the source-load-storage in each sub-microgrid.

Step 3: Calculate the generalized energy storage operation domain and the real-time net load operation point by combining equations (1) and (2), and determine whether the real-time net load operation point is in the generalized energy storage operation domain, and if so, enter step 4. Otherwise, go to step 5.

Step 4: According to the fluctuation condition of the source-load power, the ESS power output adjustment is implemented under the requirements of the fixed tie-line power control. The output characteristics should follow Fig. 3.

Step 5: According to the fluctuation condition of the source-load power, the continuous power supply and the discrete load output adjustment are performed under the requirements of the fixed tie-line power control.

Step 6: Through the output decision of the source-load-storage device in step 4 or step 5, output corresponding control commands to realize the real-time power control of the sub-microgrid.

B. MINUTE-LEVEL CENTRALIZED COORDINATED CONTROL CONSIDERING THE MAGNITUDE OF POWER CHANGE

After the island division is completed, the microgrids in each region need to make centralized optimization decisions to determine the initial allocation of source-load-storage in the region. From the mathematical point of view, the optimization decision problem has multi-constraint, discontinuous and nonlinear characteristics, which can be attributed to a mixed-integer nonlinear programming problem. To avoid the unnecessary loss due to the multi-class switching state of the storage device before and after decision, the absolute value of power change of the storage energy system is minimized.

At the same time, in the source-load-storage power optimization process of the regional multi-microgrids, it is necessary to consider the maximum recovery of PV power and loads, which can be achieved by f in equation (3). It should be noted that the three-phase microgrid can be decomposed into three virtual single-phase microgrids. The three virtual single-phase microgrids contain equivalent energy storage systems, PV systems and loads.

It is assumed that there are m PQ-type ESS in the regional multi-microgrids.

$$\min \quad F = f + \sum_{i=1}^{m} \left| P_{bs,ix} - P_{bs,i0} \right| + \sum_{i=1}^{m} \left| Q_{bs,ix} - Q_{bs,i0} \right| \tag{3}$$

where $P_{bs,ix}, P_{bs,i0}$ are the active power decision-making output and the original output of the ith PQ-type ESS. $Q_{bs,ix}, Q_{bs,i0}$ are the reactive power decision-making output and the initial output of the ith PQ type ESS.
where

$$\begin{aligned} f = -\Bigg[& \left| \sum_{n_{pvsp}} P_{pv,sp} + 3 * \sum_{n_{pvvsp}} P_{pv,vsp} \right| \\ & + \left| \sum_{n_{ldsp}} K_{ld,sp}(P_{ld,sp} + Q_{ld,sp}) \right| \\ & + 3 * \sum_{n_{ldvsp}} K_{ld,vsp}(P_{ld,vsp} + Q_{ld,vsp}) \Bigg| \Bigg] \end{aligned} \tag{4}$$

where n_{pvsp}, n_{pvvsp} represent the number of single-phase PV and virtual single-phase PV; $P_{pv,sp}, P_{pv,vsp}$ represent the output of single-phase PV and virtual single-phase PV; n_{ldsp}, n_{ldvsp} are the number of single-phase loads and virtual single-phase load; $P_{ld,sp}$, $P_{ld,vsp}$ are the active power of single-phase load and virtual single-phase load; $Q_{ld,sp}$, $Q_{ld,vsp}$ are the reactive power of single-phase load and virtual single-phase load; $K_{ld,sp}$, $K_{ld,vsp}$ are the connection state of single-phase load and virtual load (1 means connected, and 0 means unconnected).

The constraint conditions include inequality constraint and equality constraint, where the inequality constraint includes three-phase unbalance degree constraint and upper and lower limits constraints of power supply output, and the equality constraint contains the power balance constraint in three independent single-phase networks.

(1) Three-phase unbalance degree constraint:

$$\varepsilon \le 15\% \tag{5}$$

(2) Upper and lower limits constraints of power supply output:

$$\begin{cases} P_{\min bs} \le P_{bs} \le P_{\max bs} \\ Q_{\min bs} \le Q_{bs} \le Q_{\max bs} \\ P_{\min pv} \le P_{pv} \le P_{\max pv} \end{cases} \tag{6}$$

(3) Upper and lower limits constraints of the main power supply output:

$$\begin{cases} P_{vfbs,\min} \le P_{vfbs} \le P_{vfbs,\max} \\ Q_{vfbs,\min} \le Q_{vfbs} \le Q_{vfbs,\max} \end{cases} \tag{7}$$

(4) Power balance constraints in an independent single-phase network:

$$\begin{cases} P_{vfbs,x} + \sum\limits_{n_{pvx}} P_{pv,x} + \sum\limits_{n_{pvvsp}} P_{pv,vsp} + \sum\limits_{n_{bsx}} P_{bs,x} + \\ \sum\limits_{n_{bsvsp}} P_{bs,vsp} = \sum\limits_{n_{ldx}} K_{lda} P_{ld,x} + \sum\limits_{n_{ldvsp}} K_{ldvsp} P_{ld,vsp} \\ Q_{vfbs,x} + \sum\limits_{n_{bsx}} Q_{bs,x} + \sum\limits_{n_{bsvsp}} Q_{bs,vsp} = \sum\limits_{n_{ldx}} K_{lda} Q_{ld,x} \\ \qquad + \sum\limits_{n_{ldvsp}} K_{ldvsp} Q_{ld,vsp} \end{cases} \tag{8}$$

where $P_{\max bs}, P_{\min bs}, Q_{\max bs}, Q_{\min bs}$ are the upper and lower limits of active and reactive power output; $P_{bs}, Q_{vfbs,x}$ are the final active and reactive power output of ESS after centralized decision-making; $P_{vfbs,\max}, P_{vfbs,\min}, Q_{vfbs,\max}$, $Q_{vfbs,\min}$ are the upper and lower limits of active power output of main ESS; $P_{vfbs,x}, Q_{vfbs,x}$ are the active power output of phase x of the main ESS; $P_{bs,x}, Q_{bs,x}$ are the active and reactive energy output of PQ ESS in phase x; $P_{\max pv}, P_{\min pv}$ are the upper and lower limits of PV output, P_{pv} is the final output of PV after centralized decision-making, $P_{pv,x}$ is the active power output of PV in phase x; $P_{ld,x}, Q_{ld,x}$ is the active and reactive power of load in phase x.

In this way, the output of the source-load-storage of the regional multi-microgrids can be determined, and the three-phase unbalance constraints of the three-phase/single-phase hybrid structure multi-microgrids can be considered.

C. HOUR-LEVEL ISLAND COMBINATION AND ON/OFF GRID SEARCH SWITCHING

The characteristics of multi-microgrids in different combinations of sub-microgrids in a three-phase/single-phase hybrid multi-microgrids system are different. To ensure the stability and reliability of the operation of the multi-microgrids system, and to achieve the optimal configuration of the overall resources, the dynamic islanding of the regional autonomous three-phase/single-phase hybrid multi-microgrids is performed through interconnection scheme decision.

The proposed hour-level dynamic islanding strategy of the three-phase/single-phase hybrid structure multi-microgrids is shown in Fig. 6. First, a comprehensive multi-index evaluation model for multi-microgrids island operation is established, and the evaluation indicators include the stability margin of regional main power supply, regional continuous operation time and operation risk of islanding partition. Then, the islanding partition scheme of three-phase/single-phase hybrid structure multi-microgrids is solved by a discrete particle swarm optimization algorithm. Last, the combined state switching of three-phase/single-phase hybrid multi-microgrids is realized by the islanding scheme through the search and switching of combinations and splitting paths.

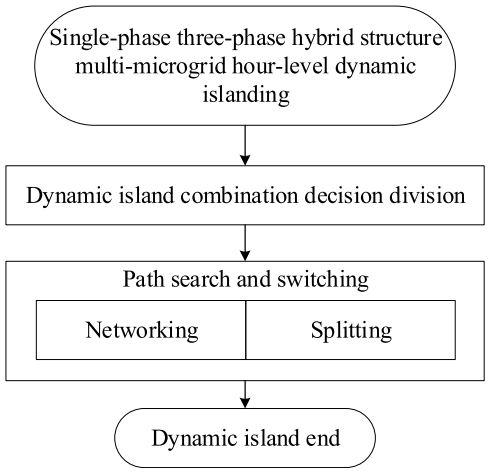

FIGURE 6. Hourly dynamic islanding process for MMGs with three-phase/single-phase hybrid structure.

1) ISLAND COMBINATION

The comprehensive multi-index evaluation model is detailed as follows:

a: STABILITY MARGIN OF REGIONAL MAIN POWER SUPPLY

Due to the loss of support of the distribution network, if the sudden drop of renewable energy power exceeds the instantaneous response capability of the main power supply in the regional microgrid, voltage and frequency of the regional microgrid will suddenly drop or even become unstable. To describe the response capability of the regional main power supply, a stability margin indicator of the regional main power supply is introduced in (9).

$$f_1=\frac{S_{BSvf\_all}-\left|S_{BSvf}\right|}{\max(|S_{PV}|,S_{PV\_all}-|S_{PV}|)+\max(|S_{LD}|,S_{LD\_all}-|S_{LD}|)} \tag{9}$$

where $S_{BSvf\_all}, S_{PV\_all}, S_{LD\_all}$ represent the rated capacity of the main power supply, rated capacity of PV and rated capacity of load in the regional microgrid, respectively; S_{BSvf}, S_{PV}, S_{LD} represent the real-time power of the main power supply, real-time power of PV and real-time power of load in the regional microgrid, respectively.

b: REGIONAL CONTINUOUS OPERATION TIME

Considering the extreme operating conditions, in which all of the intermittent power supplies are completely stopped, the continuous operation time that remaining energy of the ESS can support the load in the regional microgrid is calculated by (10).

$$f_2 = \frac{\sum(S_{BS} \times (SoC - SoC_{low}))}{S_{LD}} \tag{10}$$

where S_{BS} is the capacity of each ESS in the regional microgrid; SoC is the real-time state of charge of each ESS; SoC_{low} is the minimum allowable state of charge value of the ESS.

c: OPERATION RISK OF ISLANDING PARTITION

For different island combination plans, the number of switches that need to be operated during the island combination switching process is different, and thus the risk of operating errors is different. Therefore, the number of switching actions of the island partition scheme needs to be fully considered, which can also reflect the risk of switching states. The calculation of the operation risk of islanding partition is presented in (11).

$$f_3 = 1 - A^n \tag{11}$$

where A is the availability of the switch, n is the number of switches required to form an islanding partition scheme. It should be noted that the availability of the low-voltage switch meets specific regulatory requirements [28]. In this paper, the availability of the switch is assumed to be 0.96, since the studied autonomous multi-microgrids system can be widely applicable, especially in remote areas such as islands. Since the operational risk is positively correlated with the operational complexity, the indicator can measure the degree of risk of different partitions.

2) THE PROCESSING OF REGIONAL INDICATORS

The regional indicators are used to describe the performance of a certain aspect of a regional microgrid in an islanding partition scheme, whereas the global indicators are used to describe the performance of a particular aspect of the entire multi-microgrids. Therefore, the stability margin of regional main power supply and regional continuous operation time

are regional indicators; the operation risk of islanding partition is a global indicator. In order to achieve an overall evaluation of the islanding partition scheme, regional indicators need to be transformed into global indicators.

The stability margin of regional main power supply and regional continuous operation time are all benefit indicators. For one kind of islanding partition scheme, the smallest item in each regional microgrid is taken as the evaluation index of the islanding division, including $f_1^{\min}$ and $f_2^{\min}$. And the normalization of $f_1^{\min}$, $f_2^{\min}$ and f_3 can be calculated by (12)-(14).

$$\begin{cases} \overline{f}_1 = (f_{1,i}^{\min})/f_{1,\max}^{\min} \\ f_{1,\max}^{\min} = \max\limits_{1\le i\le n}\{f_{1,i}^{\min}\} \end{cases} \tag{12}$$

$$\begin{cases} \overline{f}_2 = (f_{2,i}^{\min})/f_{2,\max}^{\min} \\ f_{2,\max}^{\min} = \max\limits_{1\le i\le n}\{f_{2,i}^{\min}\} \end{cases} \tag{13}$$

$$\begin{cases} \overline{f}_3 = 1 - f_{3,i}/(f_{3,\max} + f_{3,\min}) \\ f_{3,\max} = \max\limits_{0<i\le n}\{f_{3,i}\} \\ f_{3,\min} = \min\limits_{0<i\le n}\{f_{3,i}\} \end{cases} \tag{14}$$

where n is the number of samples, which is equal to the number of populations in the discrete particle swarm algorithm in actual implementation; $f_{1,i}^{\min}$ is the global stability margin index of the main power supply of the ith islanding partition scheme; $f_{2,i}^{\min}$ is the global continuous operation time indicator of the ith islanding division scheme; $f_{3,i}$ is the operation risk index of the ith islanding partition scheme.

Hence, the flowchart of the islanding division algorithm for multi-microgrids is described as follows:

Step 1: Input initial data of multi-microgrids. The RMGCC collects the configuration information and real-time power of the source-load-storage in each sub-microgrid. Input the set of tie-line circuit breakers which can be operated and disconnected in this island division.

Step 2: Data Initialization. Set the initial speed v_{jm}^k; set the total number of iterations K; take the number of elements in the set of tie-line breakers as the dimension of the particle swarm M; set the initial population number of the particle swarm N. N initial M-dimensional particle swarms are randomly generated.

Step 3: Calculate the solution of M-dimensional particles x_j^k. One particle corresponds to one islanding partition scheme. Input N particles $x_1^k, x_2^k, \ldots x_N^k$ into the comprehensive evaluation model to calculate their comprehensive evaluation indexes $f_1^k, f_2^k, \ldots, f_N^k$.

Step 4: Record the position of the individual optimal solution and the position of the global optimal solution under the current iteration number.

Step 5: Determine whether the number of iterations K is reached. If so, output the position of the global optimal solution particle, which is the final island combination scheme. If not, increase K by one and go to step 6.

Step 6: Update the velocity of particles in each dimension and the position of the particle in each dimension in the next moment. Return to step 3 to calculate the solution of the M-dimensional particles.

3) NETWORKING

Fig. 7 shows the searching flowchart of the networking path for three-phase/single-phase hybrid structure multi-microgrids.

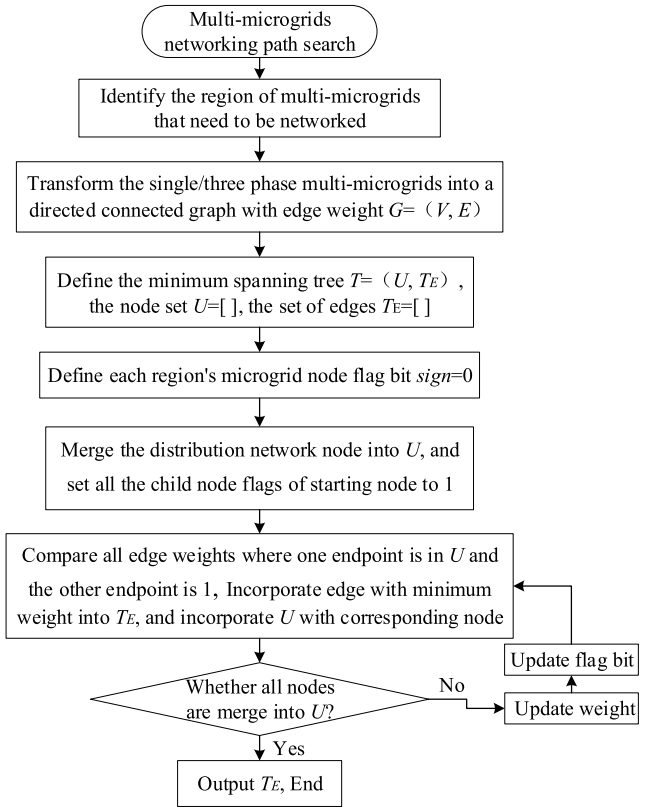

FIGURE 7. The networking path searching flowchart for MMGs with three-phase/single-phase hybrid structure.

Step 1: Identify the three-phase/single-phase hybrid structure multi-microgrids region that needs to be networked. Before the multi-microgrids connected into the distribution network, each regional microgrid RMGCC uploads its networking willingness to the RMGCC, and RMGCC determines the execution scope of the networking path search algorithm according to the intention of the microgrid interconnection in each region.

Step 2: Convert the three-phase/single-phase hybrid structure MMGs into a directed connected graph with edge weights $G = (V, E)$. The distribution network is equivalent to node 1, and each regional microgrid is equivalent to the remaining nodes. The communication path is represented by a directed edge with weights and stored in the RMGCC for identification in the form of an adjacency matrix.

Step 3: Define the minimum spanning tree of G as $T = (U, T_E)$, the initial state of the node set and the edge

set are $U = [\ ]$, $T_E = [\ ]$. The node set U of the minimum spanning tree T during algorithm execution is used to determine whether the algorithm traverses all nodes, and the edge set T_E is used to store the networked path decision result.

Step 4: Define each regional microgrid node flag bit $sign$=0. The node flag bit $sign$ is used as the basis for the node to include the weight for comparison and judgment. When $sign[j]$ is 1, it indicates that the jth regional microgrid is included in the weight comparison judgment, and is not included when it is zero. The introduction of $sign$ helps to clarify whether the layer node can be searched when searching layer by layer. Set the node flag to zero before the first search.

Step 5: To ensure the directionality and hierarchy of the networking process, the distribution network node is used as the search starting point. First, merge it into U, and set all the child node flags of the node to 1.

Step 6: Compare all edge weights where one endpoint is in U and the other endpoint is 1. Incorporate the edge with minimum weight into T_E, and incorporate U with the corresponding node. It should be noted that, when a new node is merged into U, the corresponding flag bit of the node needs to be set to zero.

Step 7: Weight update. In the actual networking process, after the regional microgrid is merged into another system through quasi-synchronous control, the voltage phase of the microgrid in that region will follow the voltage phase change of the connected system. The weight calculation is related to the phase difference between the systems. Therefore, when the new node j is merged into the node set U, the phase information of the node needs to be updated, and calculate the connectable edge weights of all nodes i to their child nodes according to the weight equation.

Step 8: Flag bit update. After the node j is selected into the node set U, all the child nodes of the node j are included in the next search range, and the corresponding flag bit is set to 1, which is consistent with the search idea of the traditional Prim algorithm.

Step 9: Return to step 6 to perform weight comparison until all nodes are merged into U, and output T_E as search result.

4) SPLITTING

The island splitting path search flowchart is shown in Fig. 8. Set $T = (U, T_E)$ as the minimum spanning tree of graph G, where U represents the set of nodes and T_E represents the set of edges of the minimum spanning tree. The edges in the T_E are sorted according to the search order. After traversing all the nodes of the graph G, T_E is the decision result of the multi-microgrids island splitting path. The search steps are elaborated as follows:

Step 1: Initial data import. The result of the islanding division of the multi-microgrids is imported into RMGCC, and RMGCC determines the execution range of the planned islanding according to the imported result.

Step 2: Convert the multi-microgrids into a connected graph with point weights $G = (V, E)$. The distribution

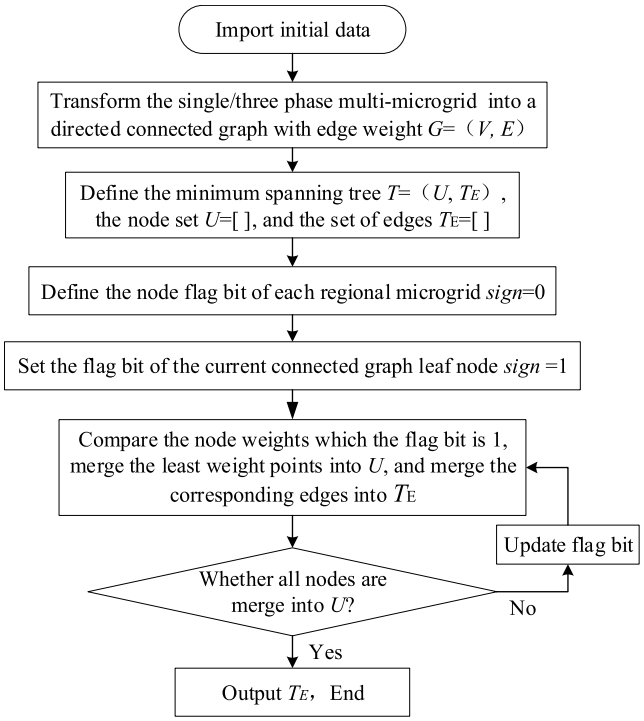

FIGURE 8. Island splitting path search flowchart.

network is equivalent to node 0, and the microgrid of each area is equivalent to the remaining nodes. The connection relationship of each node is stored in RMGCC in the form of an adjacency matrix for identification.

Step 3: Define the G minimum spanning tree $T = (U, T_E)$, and the initial state of the node set and edge set is $U = [\ ]$, $T_E = [\ ]$. The node set U of the minimum spanning tree T in the execution process of the algorithm is used to determine whether the algorithm traverses all the nodes, and the edge set T_E is used to store the decision result of the planned island splitting path.

Step 4: Define the node flag bit of each regional microgrid $sign = 0$. When $sign[j]$ is 1, it indicates that the jth region microgrid is included in the weight comparison judgment, and the microgrid is not included when $sign[j]$ is zero.

Step 5: Set the flag bit leaf node of the current connected graph to 1. The leaf node of the current connected graph is identified according to the adjacency matrix, and its flag bit is set to 1. The leaf node is the end region microgrid of the multi-microgrids.

Step 6: Compare the node weights which its flag bit is 1, merge the minimum weight points into U, and merge the corresponding edges into T_E. The flag of this node needs to be set to zero.

Step 7: Update the flag bit. When node j is selected into node set U, all parent nodes of node j are included in the next search range, and the corresponding flag bit is set to 1.

Step 8: Return to step 6 to perform weight comparison until U is merged into all nodes, and output T_E as the search result.

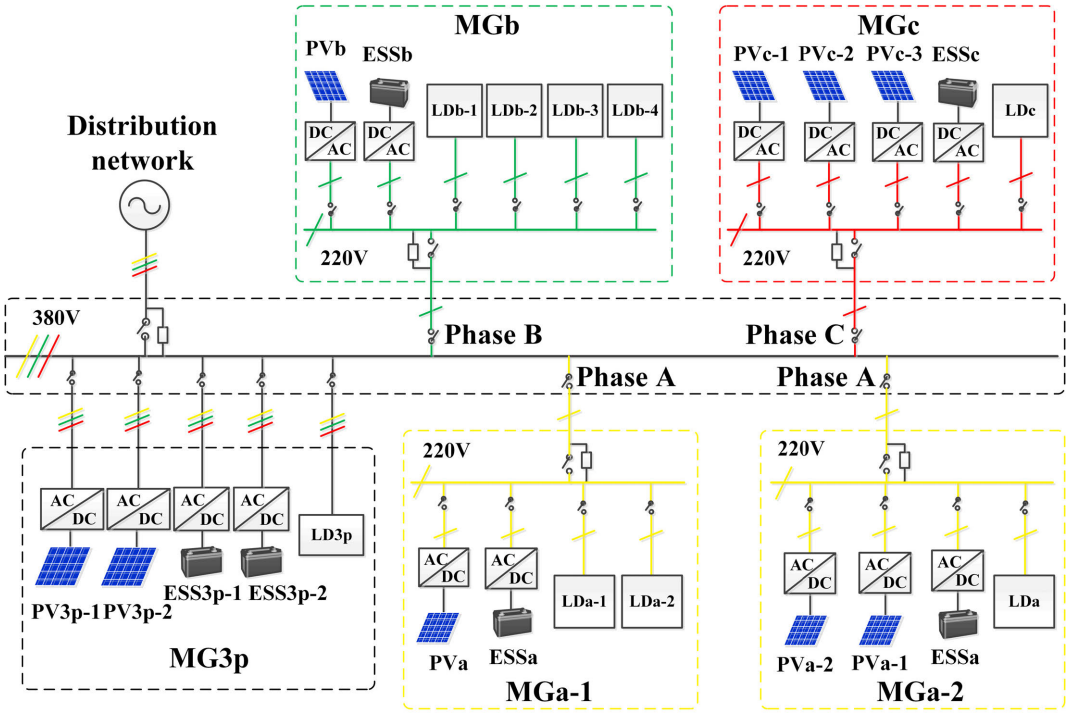

FIGURE 9. MMGs with three-phase/single-phase hybrid structure.

IV. CASE STUDIES AND DISCUSSIONS

In order to verify the effectiveness of the proposed control strategy, the multi-microgrids with three-phase/single-phase hybrid structure presented in Fig. 9 are modeled based on DIgSILENT/PowerFactory platform. The source-load-storage configuration information is shown in Table 3. The real-time information of the source, storage and load of each sub-microgrid is shown in Table 4. For brevity and clarity, MG3p denotes the three-phase sub-microgrid, MGa-1 denotes the first sub-microgrid in Phase A (A1), MGa-2 denotes the second sub-microgrid in Phase A (A2), MGb denotes the sub-microgrid in Phase B, and MGc denotes the sub-microgrid in Phase C. The switch status of the sub-microgrids MGa-1, MGa-2, MGb and MGc can be represented by "1" (closed) or "0" (open). As can be seen, the regional multi-microgrids islands are divided into 1010 (corresponding to the switch status of MGa-1, MGa-2, MGb and MGc), that is, the microgrids (MG3p, MGa-1, MGb), MGa-2, and MGc operate independently. Among them, the load 4 of the MGb is (−3 kW), and since the maximum output of the ESS of MGb is 4.5 kW (derived from equation (2)), it cannot be recovered by the second-level control.

The minute-second-hour-minute level is set to the minimum regional autonomous operation cycle process, thus to verify the proposed regional autonomous control strategy of the single-phase three-phase hybrid structure multi-microgrids. Fig. 10 shows the schematic diagram of the regional autonomy process. Each MGCC performs second-level decentralized control in real time. RMGCC performs minute-level centralized coordination optimization every 5 minutes, and performs hourly dynamic island division and gird-on/off switching every 1 hour.

TABLE 3. Sub-microgrid configuration information.

Sub-microgrid	MG3p	MGa-1	MGa-2	MGb	MGc
Phase sequence	Three phase	Phase A(A1)	Phase A(A2)	Phase B	Phase C
PV power rating /kW	30+30	5	5+5	5	5+5+5
Load rated capacity /kVA	30	4+5	5	4+5+5+5	5
ESS rated capacity /kVA	30; 30	5	5	5	5
ESS battery capacity /kWh	30; 30	5	5	5	5

TABLE 4. Real-time information of each sub-microgrid.

Sub-microgrid	MG3p	MGa-1	MGa-2	MGb	MGc
PV real-time power /kW	12; 0	3	3; 2	2	3; 2; 0
Load real-time power /kW + kVar	-21	-2; -4-1i	-2	-1-1i; -2; -3; 0	-4
ESS real-time power /kW + kVar	9; 0	3+1i	-3	4+1i	-1
ESS state /%	60	40	50	55	65

A. MINUTE-LEVEL CENTRALIZED COORDINATION

In this subsection, the centralized decision is made on the regional microgrids (MG3p, MGa-1, MGb), and the

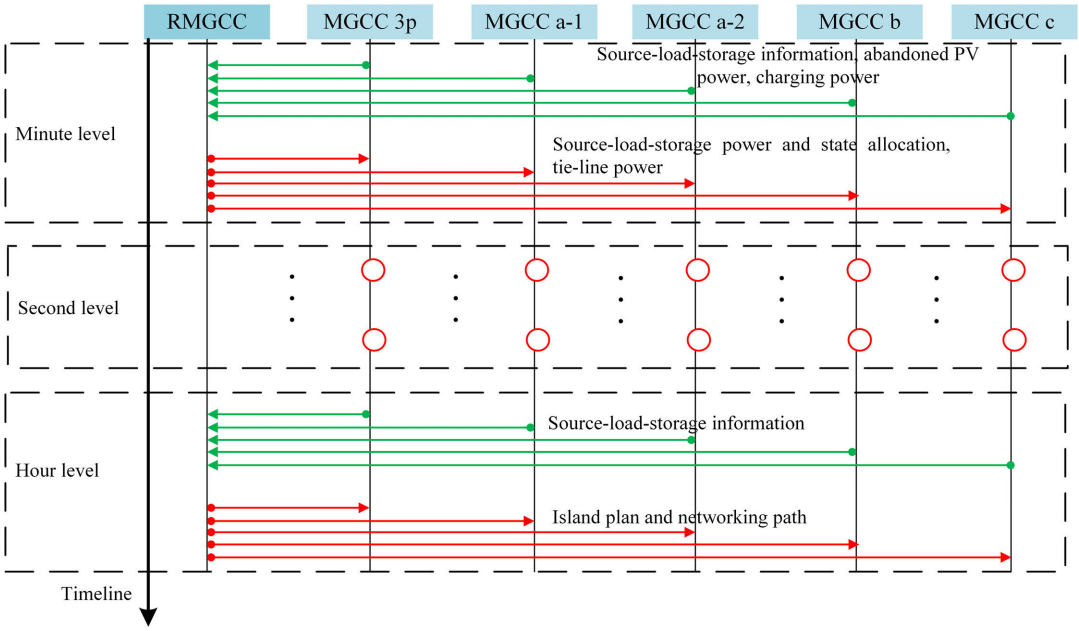

FIGURE 10. Regional autonomous strategy flow schematic.

corresponding power curves process of each device are shown in Fig. 11. As shown, the MGb load 4 (−3 kW) can be connected. Also, the output of A1 phase of the ESS is set to 2.82 kW−1.15 kVar, and the output of B phase the ESS is set to 4.39 kW. At this moment, the three-phase unbalance degree of the system is 5.43%, and the corresponding output of each phase of the three-phase VF ESS are [3.18 kW +2.15kVar; 5.61 kW +1kVar; 3 kW +0 kVar].

B. SECOND-LEVEL DECENTRALIZED CONTROL

In order to test the performance of the second-level real-time power control of the sub-microgrid presented in Section III-A, at $t = 2$ s, the power fluctuation scenarios are set and studied as follows:

(1) Assume that PV 1 in MGa-1 drops from 3 kW to 1 kW; at this moment, the SoC of the ESS is 40 %, and the upper limit of charge and discharge is [−4.5 kW 4.5 kW] obtained from equation (2), so the ESS cannot be meet the power balance requirement. Therefore, the load 1 (−2 kW) needs to be curtailed. The power curves of the device are shown in Fig. 12.

(2) Assume that PV 2 in MGa-2 is raised from 2 kW to 4 kW, and the SoC of the ESS is 50%. The upper limit of charge and discharge can be obtained by equation (2) is [−4.5 kW 4.5 kW], so the ESS outputs power of −4.5 kW, while PV 2 is set to an output of 3.5 kW. The power curves of the device are shown in Fig. 13.

(3) Assume that PV 3 in MGc is raised from 0 kW to 4 kW. At this moment, the SoC of the ESS is 65%, and the upper limit of charging by equation (2) is −3.375 kW. Therefore, PV 3 can only output power of 2.375 kW. The power curves of the device in the microgrid are shown in Fig. 14.

In the above three power fluctuation scenarios, the proposed strategy fully considers the actual operating conditions of the ESS. Moreover, it maintains the tie-line power at a given value on the basis of maximizing the source-load benefit, ensuring that the three-phase unbalance factor of the system is satisfied.

C. HOUR-LEVEL DYNAMIC ISLANDING

To thoroughly verify the gird-on/off switching performance of the dynamic island combination in the process of regional autonomy, the SoC states of MGa-1 and MGa-2 in the real-time information of the multi-microgrids are modified to 70% and 30%, respectively, and the phase information of each sub-microgrid is supplemented. The details are shown in Table 5.

TABLE 5. Sub-microgrid operating information.

Sub-microgrid	MG3p	MGa-1	MGa-2	MGb	MGc
PV real-time power /kW	12; 0	1	3; 3.5	2	3; 2; 2.375
Load real-time power /kW + kVar	-21	0; -4-1i	-2	-1-1i; -2; -3; -3	-4
Energy storage real-time power /kW + kVar	11.79+3.15i; 0	2.82-1.15i	-4.5	4.39	-3.375
Energy storage state /%	60	70	30	55	65
Phase / °	(50, -70, 170)	50	70	-70	175

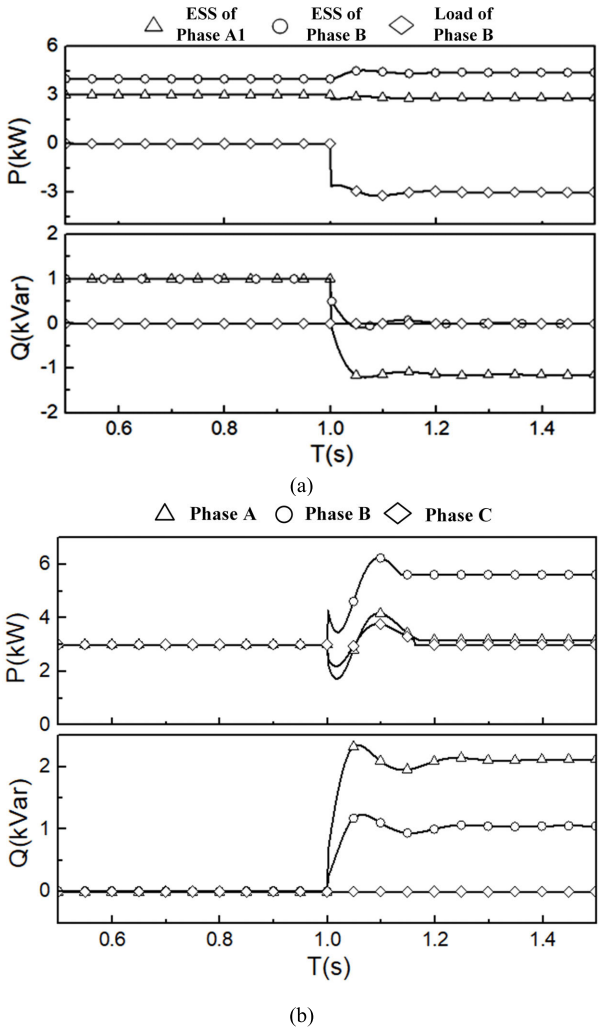

FIGURE 11. Load recovery process after centralized decision-making. (a) The power curves of regional MMGs related devices. (b) The power curves of main power phase power.

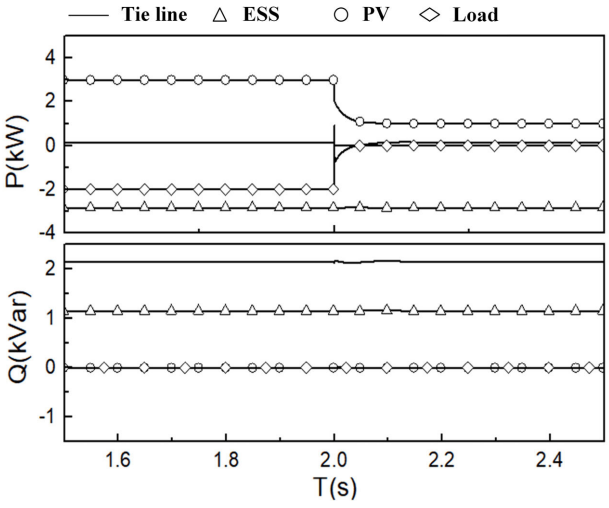

FIGURE 12. The power curves of MGa-1 devices.

The decision is implemented by the dynamic island combination strategy. The scheme is 0110, that is, the microgrids

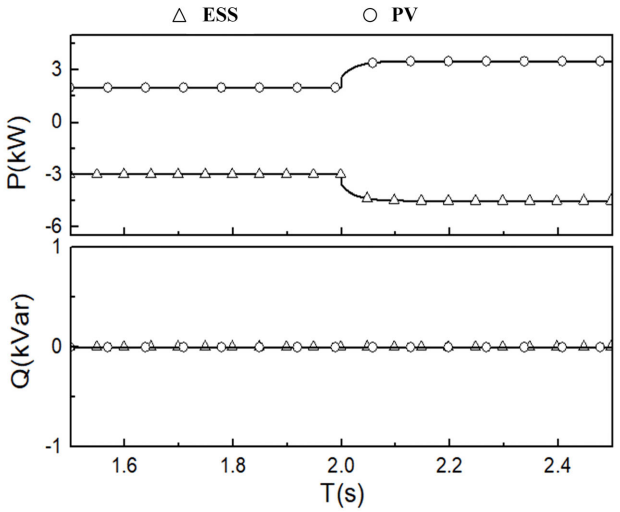

FIGURE 13. The power curves of MGa-2 devices.

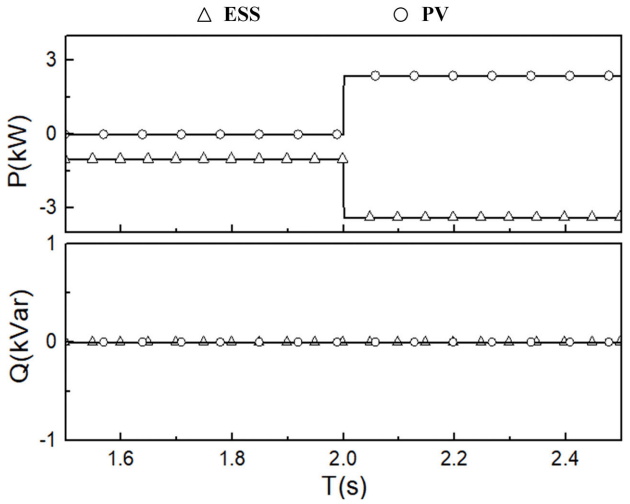

FIGURE 14. The power curves of MGc devices.

(MG3p, MGa-2, MGb), MGa-1, and MGc operate independently. MGa-1 is involved in the separation of the original regional microgrid (MG3p, MGa-1, MGb), and MGa-2 is incorporated into the regional microgrids (MG3p, MGb).

As shown in Fig. 15 and Fig. 16, during the grid-connection process of the sub-microgrid MGa-2, the A-phase bus voltage of the microgrid MGa-2 leads the phase of the A-phase voltage of the MG3p node by 20° before pre-synchronization. At $t = 3$ s, the microgrid MGa-2 receives the synchronization signal, and the frequency decreases by 0.2 Hz. When the phase deviation is less than 5° and the voltage deviation is less than 10 V during regulation, the sub-microgrid MGa-2 is successfully merged into MG3p at $t = 3.1866$ s.

The tie-line power needs to be adjusted to zero before the regional multi-microgrids is separated from the sub-microgrid MGa-1. The corresponding strategy is to set the ESS output to 3 kW+1 kVar to achieve planned islanding. As shown in Fig. 17, after the sub-microgrid MGa-1 completes the ESS output adjustment at $t = 3$ s,

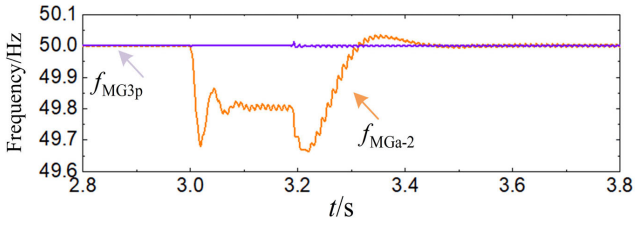

FIGURE 15. Frequency regulation process.

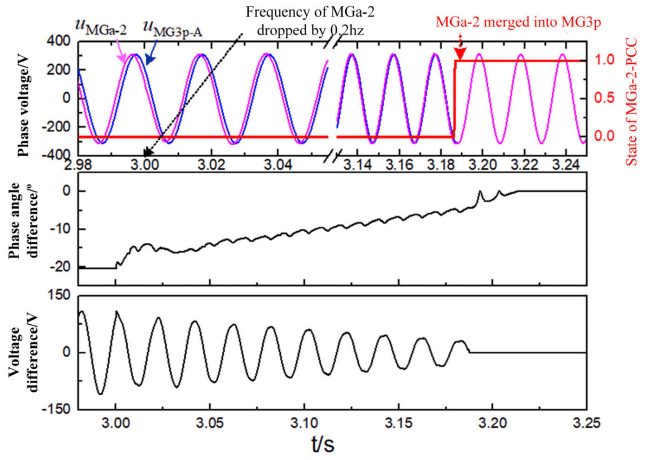

FIGURE 16. The process of MGa-2 connecting to MG3p.

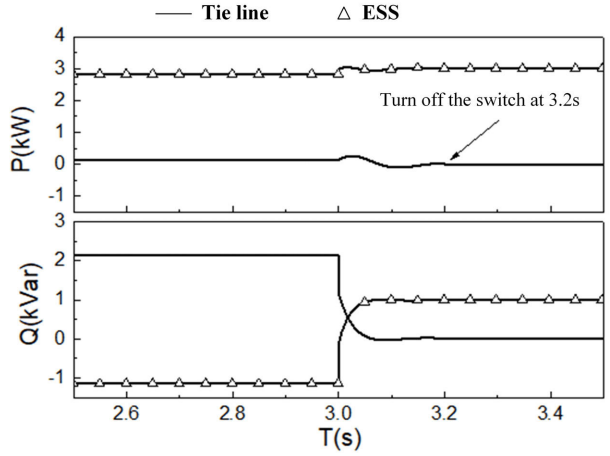

FIGURE 17. The power curves of the devices of MGa-1.

the tie-line power is zero, and islanding is achieved at $t = 3.2$ s.

D. MINUTE-LEVEL CENTRALIZED COORDINATION

At $t = 4$ s, the centralized decision on the regional microgrid (MG3p, MGa-2, MGb) is executed, and the power curves of the devices of the regional MMGs are shown in Fig. 18. As can be observed, the surplus output of PV 2 in MGa-2 (0.5 kW) can be exploited, and the output of the A2-phase ESS can be set to −4.07 kW−1.44 kVar, and the output of B-phase ESS is set to 4 kW. At this moment, the unbalance degree is 8.68%. The corresponding output of each phase of

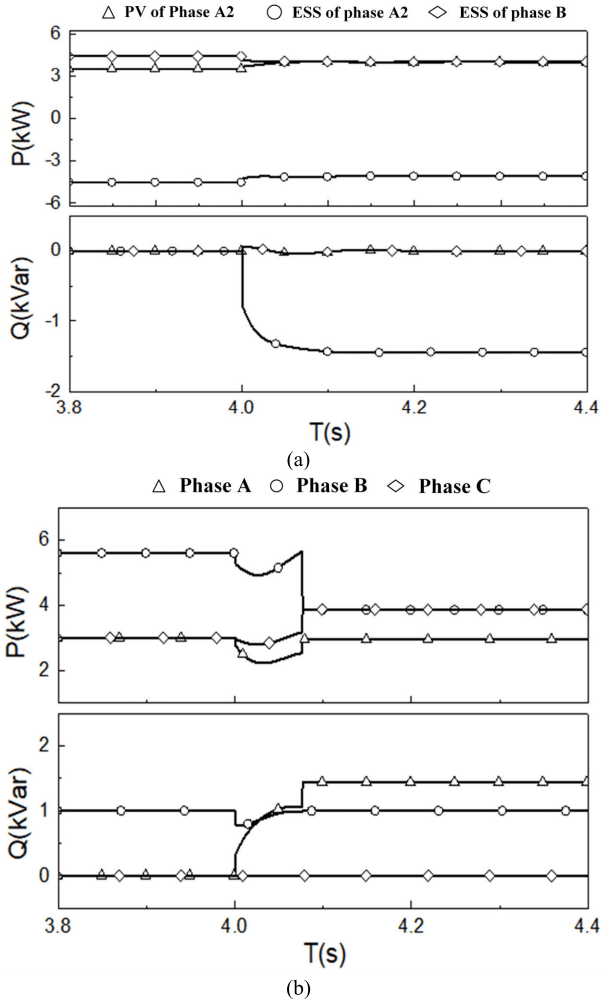

FIGURE 18. PV recovery process after centralized decision-making.
(a) The power curves of the devices of the regional MMGs.
(b) The power curves of main power phase power.

the three-phase VF ESS are [2.94 kW+1.44 kVar; 3.86 kW + 1 kVar; 3.87 kW +0 kVar].

V. CONCLUSION

Aiming at the regional autonomous multi-microgrids with three-phase/single-phase hybrid structure formed under the condition of disconnected from distribution network, a multi-time-scale regional autonomous coordinated control strategy with second-level decentralized control, minute-level centralized coordination, hour-level dynamic islands is proposed. For the second-level real-time power control of the sub-microgrid, the fixed tie-line power control needs to be implemented to ensure the global demand for the established tie-line power task. In the process of suppressing the power supply and load power fluctuations, the power characteristics and the SoC partition of the ESS are fully considered to divide the ESS operation domain. On this basis, the source-load-storage operation states are determined. For the minute-level centralized coordinated control, the maximum recovery of PV power, load and the minimum absolute value of power change of the storage energy system are selected as the

optimization objective; also, the three-phase unbalance degree is selected as the specific topology constraints, and the centralized source-load-storage power allocation control is achieved based on the mixed-integer nonlinear programming. For the hour-level island combination and on/off grid search switch, aiming at realizing the optimal allocation of regional multi-microgrids resources, the combined state switching of the three-phase/single-phase hybrid structure multi-microgrids is realized through the search and switching of combinations and splitting path by the islanding scheme.

Comprehensive verification results are presented to validate the proposed multi-time-scale regional autonomous coordinated control strategy. It is shown that coordination among the second-level decentralized control, the minute-level centralized coordination and the hour-level dynamic islanding can ensure satisfactory performance for the regional autonomous multi-microgrids with three-phase/single-phase hybrid structure under complex operation conditions.

REFERENCES

[1] R. H. Lasseter, "Microgrids," in *Proc. IEEE Power Eng. Soc. Winter Meet.*, Jan. 2002, vol. 1, pp. 305–308.

[2] S. Parhizi, H. Lotfi, A. Khodaei, and S. Bahramirad, "State of the art in research on microgrids: A review," *IEEE Access*, vol. 3, pp. 890–925, 2015.

[3] Y. Han, K. Zhang, H. Li, E. A. A. Coelho, and J. M. Guerrero, "MAS-based distributed coordinated control and optimization in microgrid and microgrid clusters: A comprehensive overview," *IEEE Trans. Power Electron.*, vol. 33, no. 8, pp. 6488–6508, Aug. 2018.

[4] Z. Xu, P. Yang, C. Zheng, Y. Zhang, J. Peng, and Z. Zeng, "Analysis on the organization and development of multi-microgrids," *Renew. Sust. Energy. Rev.*, vol. 81, pp. 2204–2216, Jan. 2018.

[5] W. Jiang, K. Yang, J. Yang, R. Mao, N. Xue, and Z. Zhuo, "A multiagent-based hierarchical energy management strategy for maximization of renewable energy consumption in interconnected multi-microgrids," *IEEE Access*, vol. 7, pp. 169931–169945, 2019.

[6] X. Dou *et al.*, "A distributed voltage control strategy for multi-microgrid active distribution networks considering economy and response speed," *IEEE Access*, vol. 6, pp. 31259–31268, May 2018.

[7] N. Pogaku, M. Prodanovic, and T. C. Green, "Modeling, analysis and testing of autonomous operation of an inverter-based microgrid," *IEEE Trans. Power Electron.*, vol. 22, no. 2, pp. 613–625, Mar. 2007.

[8] X. Guo, Z. Lu, B. Wang, X. Sun, L. Wang, and J. M. Guerrero, "Dynamic phasors-based modeling and stability analysis of droop-controlled inverters for microgrid applications," *IEEE Trans. Smart Grid*, vol. 5, no. 6, pp. 2980–2987, Nov. 2014.

[9] Z. Zhao, P. Yang, J. M. Guerrero, Z. Xu, and T. C. Green, "Multiple-time-scales hierarchical frequency stability control strategy of medium-voltage isolated microgrid," *IEEE Trans. Power Electron.*, vol. 31, no. 8, pp. 5974–5991, Aug. 2016.

[10] N. L. Díaz, A. C. Luna, J. C. Vasquez, and J. M. Guerrero, "Centralized control architecture for coordination of distributed renewable generation and energy storage in islanded AC microgrids," *IEEE Trans. Power Electron.*, vol. 32, no. 7, pp. 5202–5213, Jul. 2017.

[11] D. Wu, F. Tang, T. Dragicevic, J. C. Vasquez, and J. M. Guerrero, "A control architecture to coordinate renewable energy sources and energy storage systems in islanded microgrids," *IEEE Trans. Smart Grid*, vol. 6, no. 3, pp. 1156–1166, May 2015.

[12] M. Mohiti, H. Monsef, A. Anvari-Moghaddam, and H. Lesani, "Two-stage robust optimization for resilient operation of microgrids considering hierarchical frequency control structure," *IEEE Trans. Ind. Electron.*, early access, Dec. 5, 2019, doi: 10.1109/TIE.2019.2956417.

[13] M. Vahedipour-Dahraie, H. Rashidizadeh-Kermani, A. Anvari-Moghaddam, and J. M. Guerrero, "Stochastic risk-constrained scheduling of renewable-powered autonomous microgrids with demand response actions: Reliability and economic implications," *IEEE Trans. Ind. Appl.*, vol. 56, no. 2, pp. 1882–1895, Apr. 2020, doi: 10.1109/TIA.2019.2959549.

[14] Z. Zhao, P. Yang, Y. Wang, Z. Xu, and J. M. Guerrero, "Dynamic characteristics analysis and stabilization of PV-based multiple microgrid clusters," *IEEE Trans. Smart Grid*, vol. 10, no. 1, pp. 805–818, Jan. 2019.

[15] T. John and S. P. Lam, "Voltage and frequency control during microgrid islanding in a multi-area multi-microgrid system," *IET Gener., Transmiss. Distrib.*, vol. 11, no. 6, pp. 1502–1512, 2017.

[16] G. E. Asimakopoulou, A. L. Dimeas, and N. D. Hatziargyriou, "Leader-follower strategies for energy management of multi-microgrids," *IEEE Trans. Smart Grid*, vol. 4, no. 4, pp. 1909–1916, Dec. 2013.

[17] J. Wu and X. Guan, "Coordinated multi-microgrids optimal control algorithm for smart distribution management system," *IEEE Trans. Smart Grid*, vol. 4, no. 4, pp. 2174–2181, Dec. 2013.

[18] N. Nikmehr and S. N. Ravadanegh, "Optimal power dispatch of multi-microgrids at future smart distribution grids," *IEEE Trans. Smart Grid*, vol. 6, no. 4, pp. 1648–1657, Jul. 2015.

[19] N. Bazmohammadi, A. Tahsiri, A. Anvari-Moghaddam, and J. M. Guerrero, "Stochastic predictive control of multi-microgrid systems," *IEEE Trans. Ind. Appl.*, vol. 55, no. 5, pp. 5311–5319, Sep./Oct. 2019.

[20] N. Bazmohammadi, A. Tahsiri, A. Anvari-Moghaddam, and J. M. Guerrero, "A hierarchical energy management strategy for interconnected microgrids considering uncertainty," *Int. J. Elect. Power Energy Syst.*, vol. 109, pp. 597–608, Jul. 2019.

[21] S. A. Arefifar, M. Ordonez, and Y. A.-R. I. Mohamed, "Energy management in multi-microgrid systems-development and assessment," *IEEE Trans. Power Syst.*, vol. 32, no. 2, pp. 910–922, Mar. 2017.

[22] V.-H. Bui, A. Hussain, and H.-M. Kim, "A multiagent-based hierarchical energy management strategy for multi-microgrids considering adjustable power and demand response," *IEEE Trans. Smart Grid*, vol. 9, no. 2, pp. 1323–1333, Mar. 2018.

[23] H. Farzin, M. Fotuhi-Firuzabad, and M. Moeini-Aghtaie, "Enhancing power system resilience through hierarchical outage management in multi-microgrids," *IEEE Trans. Smart Grid*, vol. 7, no. 6, pp. 2869–2879, Nov. 2016.

[24] H. Farzin, M. Fotuhi-Firuzabad, and M. Moeini-Aghtaie, "Role of outage management strategy in reliability performance of multi-microgrid distribution systems," *IEEE Trans. Power Syst.*, vol. 33, no. 3, pp. 2359–2369, May 2018.

[25] H. Wang and J. Huang, "Incentivizing energy trading for interconnected microgrids," *IEEE Trans. Smart Grid*, vol. 9, no. 4, pp. 2647–2657, Jul. 2018.

[26] D. Gregoratti and J. Matamoros, "Distributed energy trading: The multiple-microgrid case," *IEEE Trans. Ind. Electron.*, vol. 62, no. 4, pp. 2551–2559, Apr. 2015.

[27] P. Tian, X. Xiao, K. Wang, and R. Ding, "A hierarchical energy management system based on hierarchical optimization for microgrid community economic operation," *IEEE Trans. Smart Grid*, vol. 7, no. 5, pp. 2230–2241, Sep. 2016.

[28] *IEEE Recommended Practice for Analyzing Reliability Data for Equipment Used in Industrial and Commercial Power Systems*, IEEE Standard 3006.8-2018, Oct. 17, 2018, pp. 1–71.

ZHUOLI ZHAO (Member, IEEE) received the B.S. and Ph.D. degrees from the South China University of Technology, Guangzhou, China, in 2010 and 2017, respectively.

From October 2014 to December 2015, he was a Joint Ph.D. Student (Sponsored Researcher) with the Control and Power Research Group, Department of Electrical and Electronic Engineering, Imperial College London, London, U.K. He was a Research Associate with the Smart Grid Research Laboratory, Electric Power Research Institute, China Southern Power Grid, Guangzhou, from 2017 to 2018. He is currently an Associate Professor with the School of Automation, Guangdong University of Technology, Guangzhou. His research interests include microgrid control and energy management, power electronic converters, smart grids, and distributed generation systems. He is an Active Reviewer for the IEEE TRANSACTIONS ON POWER ELECTRONICS, the IEEE TRANSACTIONS ON SMART GRID, the IEEE TRANSACTIONS ON SUSTAINABLE ENERGY, the IEEE TRANSACTIONS ON INDUSTRIAL ELECTRONICS, IEEE ACCESS, and *Applied Energy*.

ZHIRONG XU (Student Member, IEEE) received the Ph.D. degree in electrical engineering from the South China University of Technology, Guangzhou, China, in 2018.

He is currently the Integral Energy Senior Manager of the Power Wholesale Management Department, China Resources Power Holdings Company Ltd. His research interests include microgrid energy management, smart grids, and power market.

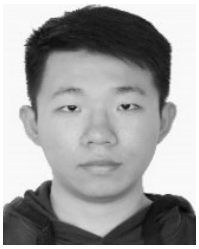

JUNTAO GUO received the B.E. degree from the Guangdong University of Technology, Guangzhou, China, in 2019, where he is currently pursuing the master's degree in electrical engineering with the School of Automation. His research interests include microgrid control and energy management.

PING YANG (Member, IEEE) received the M.S. and Ph.D. degrees in control theory and engineering from the South China University of Technology, Guangzhou, China, in 1994 and 1998, respectively.

She is currently a Professor with the School of Electric Power, South China University of Technology. She is also the Director of the National-Local Joint Engineering Laboratory for Wind Power Control and Integration Technology and the Key Laboratory of Clean Energy Technology of Guangdong Province. Her research interests include integration of renewable energy into power systems, microgrid control and management, and prediction modeling for wind and solar power.

LOI LEI LAI (Fellow, IEEE) received the B.Sc. and Ph.D. degrees from the University of Aston, in 1980 and 1984, respectively, and the D.Sc. degree from the City, University of London, in 2005.

He was the Director of the Research and Development Centre, State Grid Energy Research Institute, China; the Pao Yue Kong Chair Professor with Zhejiang University, China; and a Professor and the Chair in electrical engineering with the City, University of London. He is currently a University Distinguished Professor with the Guangdong University of Technology, Guangzhou, China. He was a member of the IEEE Smart Grid Steering Committee, the Vice President of the IEEE Systems, Man and Cybernetics Society (IEEE/SMCS), and the Fellow Committee Evaluator of the IEEE Industrial Electronics Society. He is also a member of the IEEE Smart Cities Steering Committee and a fellow of IET. He is also a National Distinguished Expert in China and a Distinguished Expert in State Grid Corporation of China. He received the IEEE Third Millennium Medal; the IEEE Power and Energy Society (IEEE/PES) UKRI Power Chapter Outstanding Engineer Award, in 2000; the IEEE/PES Energy Development and Power Generation Committee Prize Paper, in 2006 and 2009; the IEEE/SMCS Outstanding Contribution Award, in 2013 and 2014; and the Most Active Technical Committee Award, in 2016.